Available online at www.sciencedirect.com
SCIENCE DIRECT
Remote Sensing of Environment 96 (2005) 497 – 508
Remote Sensing of Environment
www.elsevier.com/locate/rse

Ecosystem structure along bioclimatic gradients in Hawai'i from imaging spectroscopy

Gregory P. Asner[a,*], Andrew J. Elmore[a], R. Flint Hughes[b], Amanda S. Warner[a], Peter M. Vitousek[c]

[a]Department of Global Ecology, Carnegie Institution of Washington, 260 Panama Street, Stanford, CA 94305, USA
[b]Institute for Pacific Islands Forestry, USDA Forest Service, Hilo, HI 96720, USA
[c]Department of Biological Sciences, Stanford University, Stanford, CA 94305, USA

Received 24 February 2005; received in revised form 8 April 2005; accepted 16 April 2005

Abstract

The Hawaiian Islands contain more than two-thirds of the life zones delineated by Holdridge, L.R., 1947. Determination of world plant formations from simple climate data. Science, 105, 367–368, and is thus an ideal testing ground for remote sensing studies of ecosystem function and structure. We tested the generality of imaging spectroscopy with "tied" red-edge and shortwave-infrared (RE-SWIR2) spectral mixture modeling for automated analysis of the lateral distribution of plant tissues and bare substrate across diverse bioclimatic gradients in Hawai'i. Unique quantities of the fractional cover of photosynthetic and non-photosynthetic vegetation (PV, NPV) and bare substrate identified fundamental differences in ecosystem structure across life zones. There was a ~20-fold increase in fractional PV cover with a 10-fold increase in mean annual precipitation ($\leq$250–2000 mm year^{-1}). This rate of increase diminished from 2000 to 3000 mm year^{-1} of rainfall, suggesting that photosynthetic canopy cover may be limited by water saturation at 3000 mm year^{-1}. The amount of exposed surface senescent material (NPV) remained nearly constant at ~50% in ecosystems with a mean annual precipitation <1500 mm year^{-1}. Thereafter, NPV steadily declined to a minimum of ~20% at 3000 mm year^{-1} of rainfall. Bare substrate fractions were highest (~50%) at precipitation levels <750 mm year^{-1}, then declined to <20% in the 750–1000 mm year^{-1} zones. The combination of low bare substrate and high NPV cover in the 750–1000 mm year^{-1} rainfall zones identified these areas as high fire risk. Remotely sensed fractional cover of PV+NPV was poorly correlated with canopy leaf area index (LAI), showing the uniqueness of the lateral structural measurement afforded by automated RE-SWIR2 spectroscopy approaches. The results indicate the accuracy, precision and applicability of imaging spectroscopy for ecological research across a wide range of bioclimatic conditions.

Keywords: AVIRIS; Hyperspectral; Non-photosynthetic vegetation; Remote sensing; Shortwave-infrared radiation; Spectral mixture analysis; SWIR

1. Introduction

The Hawaiian Archipelago contains volcanic terrain features that result in an unusual diversity of environmental conditions, with rainfall gradients spanning ~180–11,000 mm and mean annual temperatures ranging from ~5 to 27 °C (Armstrong, 1983; Giambelluca et al., 1986). An enormous range of ecological conditions occurs along these gradients. Of the Hawaiian Islands, the "Big Island" of Hawai'i alone contains 25 of the 35 the global life zones delineated by Holdridge (1947) (Fig. 1). Humid rain forest, mesic woodlands and shrublands, arid grasslands, and alpine tundra are common along elevational gradients on five volcanoes. These life zones are dissected by a mosaic of lava flows of differing ages, which define stages of soil and ecosystem development (Vitousek et al., 1992). Hawai'i also contains an expanding mosaic of invasive plants in many of the native ecosystems that span these environmental gra-

* Corresponding author. Tel.: +1 650 462 1047x200; fax: +1 650 462.
E-mail address: gpa@stanford.edu (G.P. Asner).

0034-4257/$ - see front matter © 2005 Elsevier Inc. All rights reserved.
doi:10.1016/j.rse.2005.04.008

Fig. 1. Holdridge (1947) life zone map of Hawai'i with field sites shown in orange triangles. Geographic coverage of AVIRIS imaging spectrometer observations is shown in red boxes.

dients. This combination of varying bioclimatic, edaphic and taxonomic factors provides an environmentally diverse setting to develop remote sensing theories and methods pertaining to ecosystem structure, function and disturbance.

Optical remote sensing is central to regional and global analyses of vegetation physiological properties and land cover. Remote sensing of physiology focuses on functional attributes of vegetation such as fractional photosynthetically active radiation absorption (Field et al., 1995; Sellers, 1985). This type of remote sensing often employs multi-spectral vegetation indices, including the normalized difference vegetation index (NDVI), as spatial and temporal indicators of physiological properties. Multi-spectral remote sensing is also commonly used with statistical classification approaches to estimate the extent of land covers such as forest, grassland, and urban areas (review by Franklin & Wulder, 2002).

In comparison to physiological and land cover applications, a less common but growing area in remote sensing is that of ecosystem structural analysis. Remote sensing of ecosystem structure is the study of the spatial distribution of biological materials in three-dimensional space. It is not a wholly new practice; aerial photography has been widely used to estimate the abundance and spatial density of trees, two important components of ecosystem structure.

Some new structural remote sensing technologies, such as laser detection and ranging (LIDAR; Lefsky et al., 1999) and interferometric synthetic aperture radar (InSAR; Treuhaft & Siqueira, 2000), measure the vertical distribution of foliage. However, another important ecosystem structural measure is the lateral surface configuration of biological materials. The surface heterogeneity of live, senescent and detrital materials indicates the partitioning of many biogeochemical processes such as the fixation, decomposition, and storage of carbon (Aber & Melillo, 1991; Schlesinger, 1991). Imaging spectroscopy is not often considered a structural remote sensing technology, but recent advances in signal processing have isolated the fractional cover of biological materials while minimizing effects that cause other remote sensing techniques to be simultaneously sensitive to cover and volume (Asner & Lobell, 2000). Imaging spectroscopy may be an approach for measuring the lateral distribution of these materials on an automated basis (Asner & Heidebrecht, 2002), yet no multi-biome characterization studies have been performed because the appropriate technology is primarily aircraft-based and thus difficult to apply over large regions.

The Island of Hawai'i provides a unique opportunity to test remote sensing measurements of ecosystem structure across a significant range of vegetation types and environmental conditions. We present the first large-scale,

high spatial resolution experiment designed to evaluate how well imaging spectroscopy can measure the lateral component of ecosystem structure across bioclimatic gradients available throughout Hawai'i. As well, we used the remote sensing observations to study climate controls over fractional material cover, as baseline indicators of ecosystem conditions in Hawai'i. In doing so, we tested the efficacy of a fully automated approach for quantifying the lateral or fractional cover of live and senescent or dead plant tissues—measures considered central to landscape, regional and global studies of ecosystem structure and disturbance.

2. Methods

2.1. Remote sensing data

Imaging spectroscopy is the measurement of solar radiation reflected from the Earth's surface in contiguous, narrow spectral channels spanning the wavelength region from 0.4 to 2.5 μm. The NASA Airborne Visible and Infrared Imaging Spectrometer (AVIRIS; Green et al., 1998) was recently upgraded and is one of the few high performance imaging spectrometers available to the scientific community. AVIRIS acquires optical radiance data in 224 optical channels ranging from 0.38 to 2.5 μm with a nominal 10 nm sampling (full-width at half maximum). In October and November of 2001, AVIRIS data were collected over Hawai'i by an ER-2 (U-2) aircraft modified to fly at an altitude of ~10 km above sea level. Surface elevations within AVIRIS flight lines ranged from 0 to 2200 m, resulting in ground instantaneous field of view (pixels) ranging from 7.8 to 10.0 m. The total area imaged in this study was 1445 km^2 in 13 AVIRIS flight lines and more than 17.8 million spectral measurements (Table 1). We imaged 16 of the 25 Holdridge life zones found on the island, which spanned a mean annual precipitation range of ≤250 to ≥3000 mm (Fig. 2). Flight lines were oriented for best coverage of tropical forest, woodland, savanna, shrubland and grassland (Table 1).

The aircraft global positioning system (GPS) provided a preliminary geo-correction of the AVIRIS data. Further geo-rectification was performed using USGS digital orthophotoquad maps and geographic information system (GIS) coverages provided by the State of Hawai'i (http://www.state.hi.us). The undulating terrain introduced non-linear effects on the geometric quality of the data. These effects were compensated for by non-linear rubber sheeting of the imagery to reference GIS layers (Wiemker et al., 1996). The AVIRIS data were corrected to apparent surface reflectance to minimize the effects of water vapor and other atmospheric constituents. This step was performed using the ACORN code (ImSpec LLC, Palmdale, CA), which uses MODTRAN-4 radiative transfer modeling to estimate water vapor on a pixel-by-pixel basis. The wavelength regions used for water vapor retrieval were centered on the 940 and 1130 nm features, and a typical humid tropical atmosphere was selected for the MODTRAN simulation. No ground targets were used for image calibration.

Table 1
Imaging spectrometer observations throughout Hawai'i, summarized by Holdridge life zone and mean annual precipitation zone

AVIRIS flight line	Total area (km^2)	Holdridge life zone (% of area)	Precipitation zones (mm) (% of area)
B02	107	Lower montane wet forest (21%) Lower montane moist forest (60%) Lower montane dry forest (1%) Montane wet woodland/forest (13%) Montane moist woodland/forest (6%)	1500 (31%) 2000 (51%) ≥3000 (18%)
B03	205	Sub-tropical moist forest (2%) Sub-tropical dry forest (5%) Lower montane moist forest (10%) Lower montane dry forest (48%) Lower montane thorn steppe (20%) Montane moist woodland/forest (7%) Montane steppe (6%)	<500 (32%) 500 (43%) 750 (17%) 1000 (8%)
B05, B06	286	Lower montane moist forest (1%) Lower montane dry forest (31%) Lower montane thorn steppe (31%) Montane moist woodland/forest (9%) Montane steppe (26%) Sub-alpine moist forest (3%)	<500 (70%) 500 (30%)
B07	43	Sub-tropical wet forest (3%) Sub-tropical moist forest (82%) Lower montane moist forest (16%)	1000 (41%) 1500 (59%)
B08	141	Sub-tropical wet forest (1%) Sub-tropical moist forest (52%) Lower montane moist forest (48%)	1000 (100%)
B09, B10, B11	331	Tropical thorn forest (11%) Tropical desert bush (5%) Sub-tropical moist forest (7%) Sub-tropical dry forest (59%) Sub-tropical thorn forest (3%) Lower montane moist forest (3%) Lower montane dry forest (12%)	≤250 (16%) 500 (60%) 750 (15%) 1000 (9%)
A02	96	Tropical dry forest (2%) Tropical thorn forest (4%) Sub-tropical moist forest (22%) Sub-tropical dry forest (50%) Sub-tropical thorn forest (20%) Lower montane moist forest (2%)	500 (6%) 750 (39%) 1000 (34%) 1500 (21%)
A03	61	Lower montane rain forest (100%)	2000 (38%) ≥3000 (62%)
A05	67	Montane wet forest (100%)	2000 (81%) ≥3000 (19%)
A19	108	Montane wet forest (64%) Montane rain forest (36%)	2000 (19%) ≥3000 (81%)
TOTAL	1445		

AVIRIS flight lines are shown on Figs. 1 and 2.

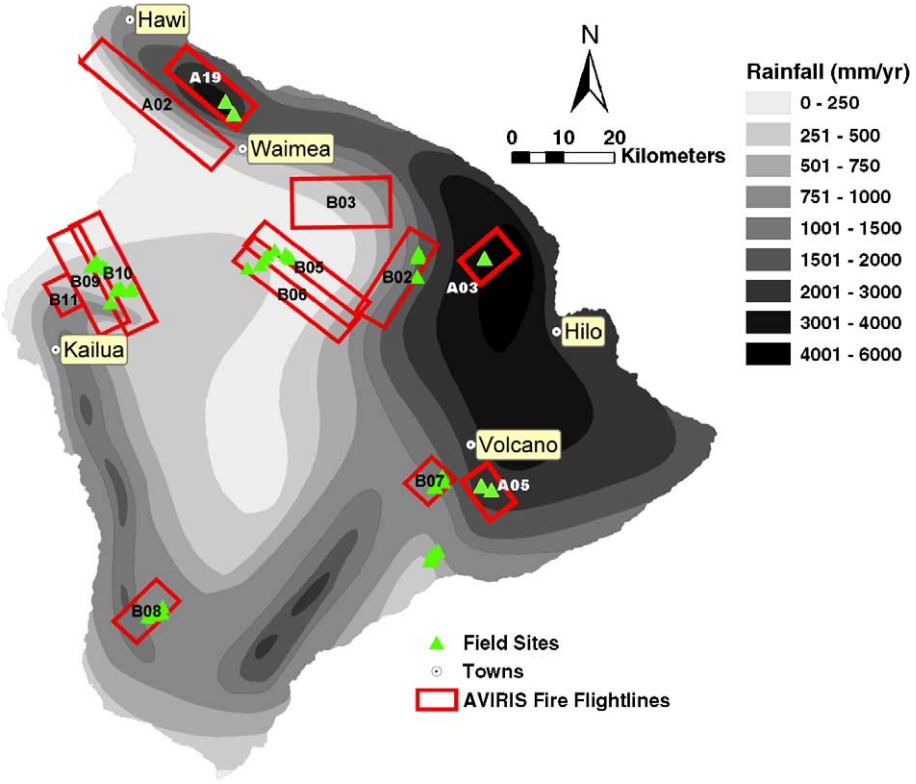

Fig. 2. Mean annual precipitation throughout the Island of Hawai'i with field sites shown in green triangles. Geographic coverage of AVIRIS imaging spectrometer observations is shown in red boxes.

2.2. Fractional cover analysis

The fractional cover of three dominant surface materials found in ecosystems – photosynthetic vegetation (PV), non-photosynthetic vegetation (NPV), and bare substrate – was quantified in each AVIRIS image pixel using a fully automated spectral unmixing algorithm designed for use with high-fidelity imaging spectrometer observations (Fig. 3). PV is comprised of live green foliage; NPV is a combination of surface litter, standing senescent material and woody surfaces exposed to the field-of-view of the imager. Bare substrate is a third surface constituent

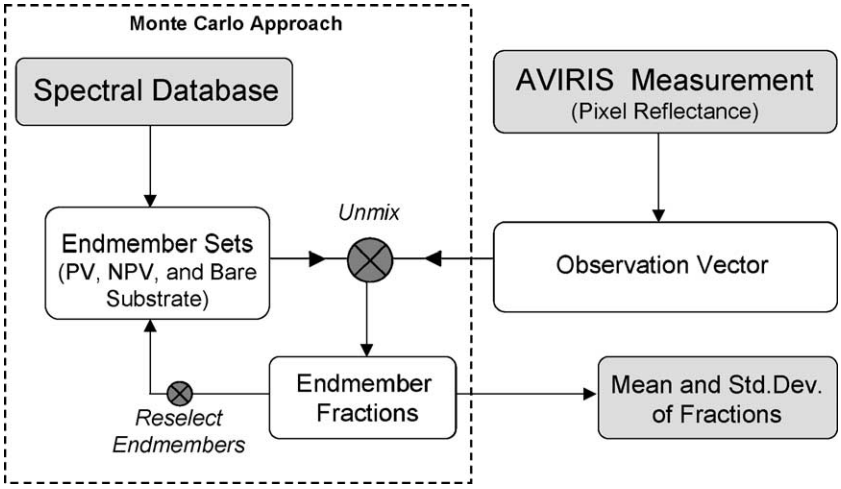

Fig. 3. Schematic of automated Monte Carlo unmixing (AutoMCU) algorithm used to analyze imaging spectroscopy data (Asner & Lobell, 2000). Each AVIRIS pixel forms an observation vector (top right). Field-based hyperspectral reflectance bundles of photosynthetic vegetation (PV), non-photosynthetic vegetation (NPV) and bare substrate are inputs to the model (top left). Random selections of these spectral endmembers (ρ_{pv}, ρ_{npv}, ρ_{s}) are used to decompose each AVIRIS pixel using Eq. (1). The procedure is repeated until a stable mean and standard deviation is achieved for each surface constituent.

representing bare soil, ash, and lava. Each of these component endmembers contributes to the pixel-level AVIRIS reflectance ($\rho(\lambda)_{\text{pixel}}$):

$$\rho(\lambda)_{\text{pixel}} = \sum_{e=1}^{n} [C_e \cdot \rho_e(\lambda)] = \left[C_{\text{pv}} \cdot \rho_{\text{pv}}(\lambda) + C_{\text{npv}} \cdot \rho_{\text{npv}}(\lambda) + C_s \cdot \rho_s(\lambda)\right] + \varepsilon(\lambda) \sum_{e=1}^{n} [C_e] = 1 \quad (1)$$

where $\rho_e(\lambda)$ is the reflectance of each land cover endmember e at wavelength λ, C is the fraction of the pixel composed of e, and $\varepsilon(\lambda)$ is the error of the solution at wavelength λ. The second equation indicates that the endmembers are forced to sum to unity.

Linear spectral mixture analysis is not new; previous efforts have proven the value of the approach in quantifying the fractional cover of vegetation types in ecosystems (e.g., Adams et al., 1993; Roberts et al., 1993). To date, most linear mixture modeling approaches have been manually executed, as spectral endmembers ($\rho_e(\lambda)$) are selected to maximize the separation of spectrally-distinct species or materials (e.g., Bateson & Curtiss, 1996). However, manual mixture analyses are limited in their generality for large-scale, high-spatial resolution studies requiring automated techniques. For this reason, spectral mixture analysis has not often been used beyond the geographic scale of landscapes or small regions. Moreover, previous mixture modeling approaches with imaging spectrometer data use the full (or nearly full) reflectance spectrum. Linear mixture models using standard reflectance data (be it hyperspectral or multi-spectral) under-determine fractional cover since multiple scattering also contributes to the measured reflectance spectrum. As such, these approaches cannot separate the effects of changes fractional cover from that of changing canopy volume or leaf area index (LAI) (Carlson and Ripley, 1997).

For automated spectral mixture analysis of the fractional cover of biological materials, successful use of Eq. (1) requires that endmember signatures ($\rho_e(\lambda)$) be general in spectral information content, yet spectrally unique and highly repeatable. They must be mostly sensitive to changes in the lateral fractional cover of the materials, and less sensitive to changes in species composition, canopy leaf area index (LAI), and biomass. Insufficient spectral separability between endmembers, or high endmember variability caused by changes in leaf chemistry or leaf volume, results in inaccurate measurements of surface cover fractions (C_e). Asner (1998) quantified the spectral separability and variability of PV, NPV and bare soil across a wide range of species, growthforms, biochemistries, and geochemistries in arid, mesic and humid ecosystems. The study suggested that the shortwave-infrared region between 2.0 and 2.4 μm (known as the "SWIR2") is spectrally the most consistent for defining PV, NPV and bare soil covers. By anchoring or tying the SWIR2 spectra at a starting point of ~2.0 μm, spectral variability is greatly reduced within each endmember while maintaining their inherent spectral uniqueness. These tied SWIR2 spectra were highly sensitive to small variations in the sub-pixel fractional cover of PV, NPV and bare soil in an arid ecosystem (Asner & Lobell, 2000). However, it was later found that the atmospheric CO_2 absorption near 2.05 μm led to uncertainty in the SWIR2 mixture modeling approach. In particular, sub-optimal atmospheric correction for CO_2 resulted in spectral confusion of PV and NPV using the tied SWIR2 spectral region alone. Asner and Heidebrecht (2002) addressed this issue by adding 0.70–0.73 μm "red-edge (RE)" spectra to Eq. (1), tying these spectra at 0.70 μm. Although the revised tied RE-SWIR2 approach was found to be precise and accurate for materials in arid grasslands and shrublands (Asner & Heidebrecht, 2002), the generality of the method remained

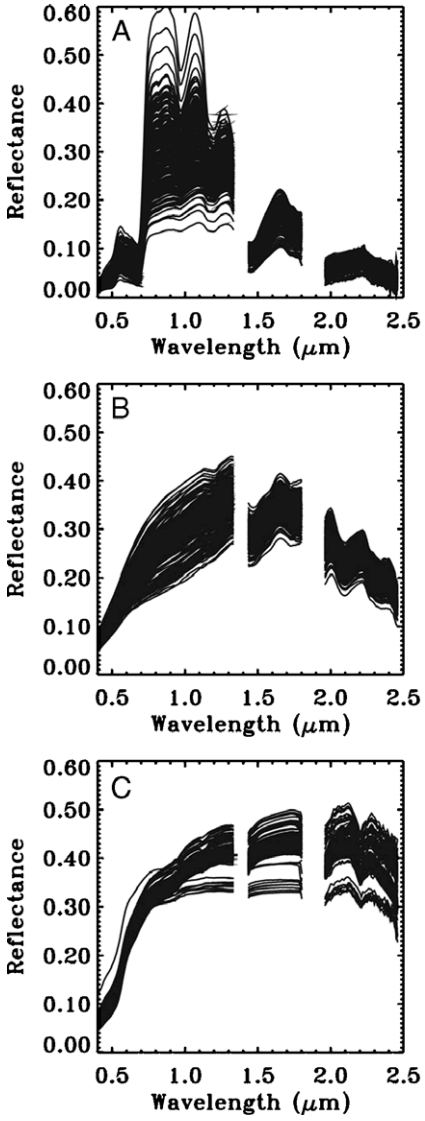

Fig. 4. Full-range reflectance spectra of photosynthetic vegetation – PV, non-photosynthetic vegetation – NPV, and bare substrate compiled from sites in North America, South America and Hawai'i.

unknown. The present study is thus designed to utilize the diverse bioclimatic gradients in Hawai'i to assess the value of the tied RE-SWIR2 method for isolating the fractional surface cover of biological and bare substrate materials.

For this study, endmember bundles for PV, NPV and bare substrate ($\rho_{pv}(\lambda)$, $\rho_{npv}(\lambda)$, $\rho_s(\lambda)$) were constructed from general field spectral databases collected in ecosystems throughout North and South America (Asner, 1998; Asner et al., 2004) and Hawai'i (this study) (Fig. 4). The spectra were tied at 0.70 μm for the red-edge and 2.03 μm for the SWIR2 portions of the spectrum to isolate the shapes of the PV, NPV and bare substrate spectra (Fig. 5). All wavelength values outside of the red-edge and SWIR2 range were discarded. Variation in endmember reflectance spectra necessary to model pixel reflectance was propagated to the sub-pixel cover fraction estimates via a Monte Carlo algorithm (Fig. 3). Endmember spectra were randomly selected from each endmember bundle (Fig. 5) and surface cover fractions were calculated (Eq. (1)); this was repeated 50 times to derive a distribution of fractions for each endmember (C_e; Fig. 3).

2.3. Field studies

During and after the AVIRIS campaign, we conducted field studies of surface properties including fractional PV, NPV and bare substrate cover and LAI. The field studies were distributed among areas of varying herbaceous and woody cover, biomass and species composition. The selected array of sites allowed us to validate the spectral mixture modeling in grasslands, shrublands, savanna, woodlands, and humid tropical forest.

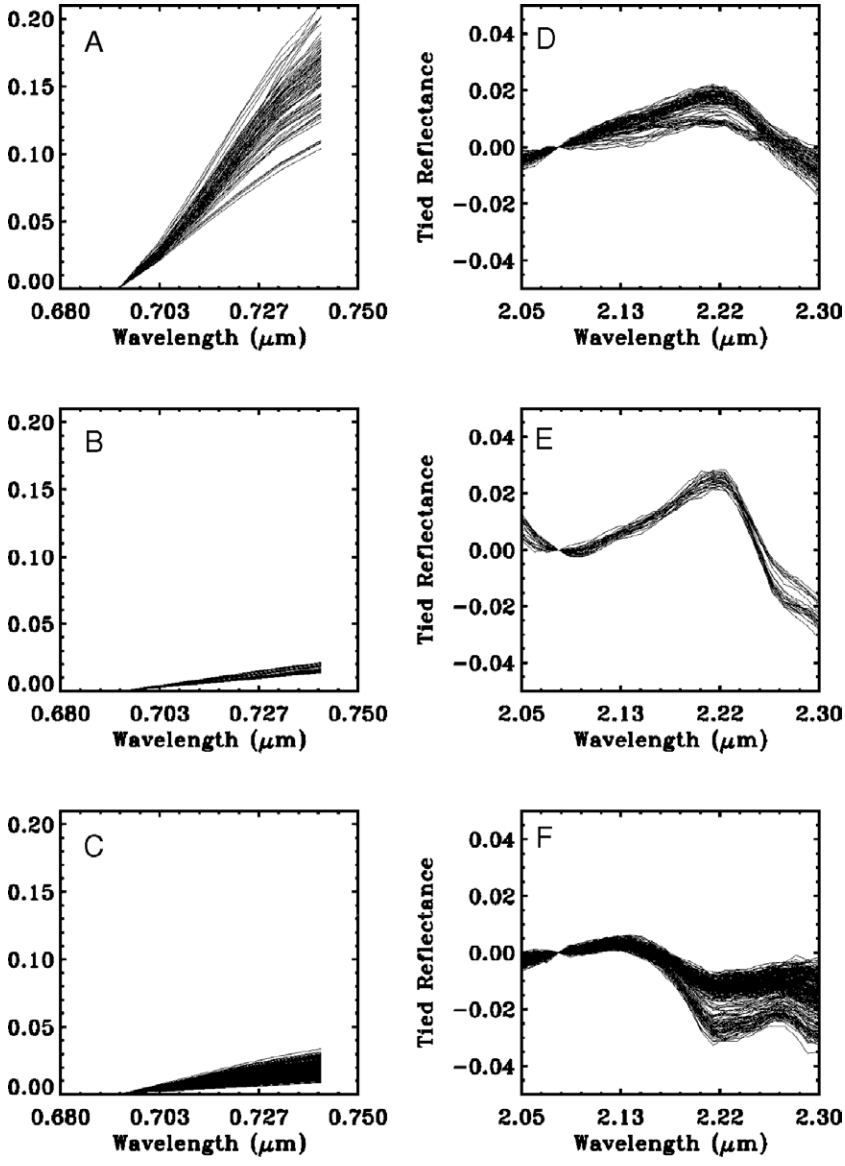

Fig. 5. Tied spectral endmember bundles used for the AutoMCU analysis. Panels A–C show tied red-edge spectra for photosynthetic vegetation – PV, non-photosynthetic vegetation – NPV, and bare substrate. Panels D–F show tied SWIR2 spectra.

At each grassland, shrubland, and savanna field site, 8–12 transects of 50 m length were selected in random compass orientations. The fractional cover of PV and NPV was determined using both line intercept and visible/near-infrared digital photography. The line intercept method was employed at 10 cm spatial resolution (Canfield, 1941), and then aggregated to 9 m AVIRIS spatial sampling. The top-of-canopy digital photography used an Agricultural Digital Camera (Tetracam Inc., Chatsworth, CA) mounted 2.5 m above the ground in the downward nadir-viewing position from a portable boom, yielding an image field-of-view of 1.5×2.5 m and a spatial resolution of approximately 2 cm. The camera uses visible and near-infrared filters to isolate the fractional cover of PV and NPV, as described in detail by White et al. (2000). Samples were collected every 5 m and analyzed using the BRIV-32 fractional cover analysis package (Tetracam Inc., Chatsworth, CA).

In woodland and forest ecosystems where canopy access was limited from the ground, helicopter flights were scheduled in the months to follow the AVIRIS data acquisitions. At approximately 100 m above the top of the canopy, the near-infrared digital camera with a zoom lens was used to collect data in 15×25 m areas at a spatial resolution of 4 cm. The data were analyzed for PV, NPV and bare soil fractions using the BRIV-32 software package. All field transects and helicopter-based digital image acquisitions were geo-located using a global positioning system with post-processing differential correction.

LAI was measured every 5 m along the 50 m transects in grasslands, shrublands, and savannas using a plant canopy analyzer (LAI-2000, Licor, Inc.). LAI was also collected on the ground at points in woodland and forest areas coincident with helicopter-based photographs. Measurements were collected under diffuse sky conditions, as required by the instrument design (Welles & Norman, 1991). A one-quarter optical block was used to remove the operator from the instrument field-of-view.

2.4. Analysis by life zone

To combine and synthesize the average climatological conditions of Hawai'i into biologically meaningful categories, we employed the life-zone equations of Holdridge (1947). We obtained geographic information system (GIS) coverages of elevation and mean annual precipitation from the Hawai'i State government (http://www.state.hi.us). The GIS elevation coverage was converted to an estimate of mean annual temperature in the following way. Ocean temperature around Hawai'i ranges from 23.3 to 26.7 °C annually (www.nodc.noaa.gov). We used 25 °C as a mean sea level temperature and a lapse rate for Hawai'i of 0.548 °C/100 m (Armstrong, 1983) to calculate isotherms from elevation contours. We then grouped these isotherms by Holdridge temperature ranges: 0–3 °C (alpine), 3–6 °C (sub-alpine), 6–12 °C (montane), 12–18 °C (lower montane), 18–24 °C (sub-tropical), and >24 °C (tropical). The derived GIS coverages of mean annual precipitation and temperature were then intersected and used to create the life zone classifications using the equations of Holdridge (1947). The resulting map is shown in Fig. 1. The mean and standard deviation of the remote sensing results (PV, NPV, bare substrate) were calculated for all pixels falling into a particular life zone throughout the AVIRIS image data set (Table 1). We acknowledge the coarse nature of the Holdridge Life Zone classification scheme, yet we found it valuable as a general organization tool for the enormous image data set collected in this study. A detailed study of available vegetation maps did not produce a better organizational method. In fact, we are working on such a map presently.

3. Results and discussion

3.1. Regional trends

Results for PV, NPV and bare substrate fractional cover for two of the AVIRIS flight lines are shown in Fig. 6. The results for the entire image set (Fig. 1) spanned the entire range of possible values, from zero to full cover, and

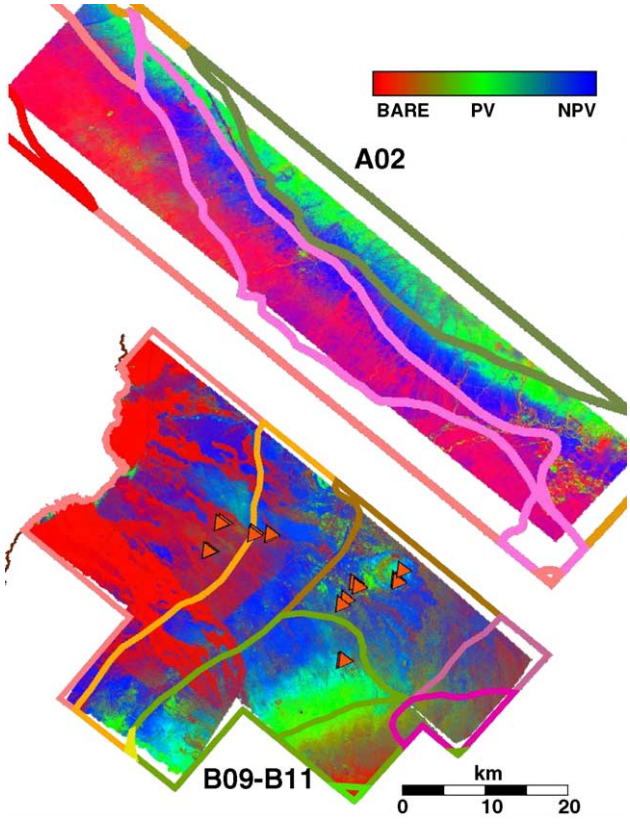

Fig. 6. Example mosaics of 9×9 m AVIRIS results following AutoMCU spectral mixture analysis. Color gradations of blue, green, and red indicate fractional abundance of NPV, PV, and bare substrate, respectively. Holdridge life zone boundaries and field sites (red triangles) are also shown as examples.

displayed regional trends with topographic slope and aspect. The lowest and highest elevations typically contained the highest levels of exposed substrate (red tones, Fig. 6). Highest elevations, such as on the upper slopes of Mauna Kea (flightlines B02–B06) and Mauna Loa (B08), were volcanic cone areas with little plant growth. Lowest elevations on the leeward side of Kohala volcano (A02) were arid ecosystems containing exposed soil and rock. In flightline B07, recent lava flows from Kilauea volcano left much of the imaged area in bare a'a and pahoehoe lava fields. The lowest elevations in Pu'u Wa'awa'a Ranch (B09–B11) were a combination of lava flow and a recent grassland fire.

The highest PV fractions were often found at mid to upper elevation, such as in the forests of Kohala (A02), Pu'u Wa'awa'a (B09–B11) and HAVO (A05) (Figs. 1 and 6). The mid-flank area of Mauna Loa (B08) also contained high PV cover fractions indicative of tropical montane forest woodlands. On the windward side of Mauna Kea (B02–B03), lower elevations had the highest PV or forest cover fractions. These were areas dominated by a mix of endemic *Metrosideros polymorpha* and plantation (e.g., tropical ash) forests.

Lower to mid-elevation zones of many AVIRIS flightlines were dominated by NPV cover (blue tones, e.g., Fig. 6). Field visits indicated that most NPV-dominated areas were comprised of grass covers, which were usually dominated by introduced species of African origin. These "NPV belts" are considered fire prone (D'Antonio & Vitousek, 1992), and they are often adjacent to woodlands containing many native species of high conservation value (Hughes et al., 1991) (green tones, e.g., Fig. 6).

3.2. Field validation

RE-SWIR2 spectral mixture analysis showed excellent quantitative performance across a large range of grassland, shrubland, savanna, woodland and rain forest conditions (Fig. 7). PV fractions were estimated with a precision (r^2) of 0.93 (Fig. 7a), while NPV fractions were slightly less precise at 0.89 (Fig. 7b) ($p<0.05$). PV was underestimated by ~2% at very low levels and was over-estimated by up to 10% at the highest values. NPV was accurately estimated at low values, but errors increased to a maximum of 13% at high values. Bare substrate was well modeled, with an $r^2=0.92$ ($p<0.01$).

The single largest source of error in the tied RE-SWIR2 unmixing approach is that of pronounced substrate chemical variation, and this Hawai'i study spanned an enormous range of substrate conditions, including bare a'a and pahoehoe lava flows, volcanic ash, recently burned (blackened) soils, and oxic clays. Some inaccuracies could well be due to variation in substrate types unaccounted for in the endmember reflectance bundles (Fig. 5).

In addition to substrate-spectral reflectance uncertainties, there were errors in comparing results from field and remotely sensed measurements. Asner and Heidebrecht (2003) found that image-to-field colocation errors alone accounted for nearly 20% of the total uncertainty in remotely sensed PV and NPV results. These errors would thus account for all of the uncertainty in the Hawai'i study. Nonetheless, these validation studies confirmed the efficacy of tied RE-SWIR2 imaging spectroscopy an approach for automated large-scale, high-resolution analysis of vegetation structure across a wide range of ecosystem types and conditions.

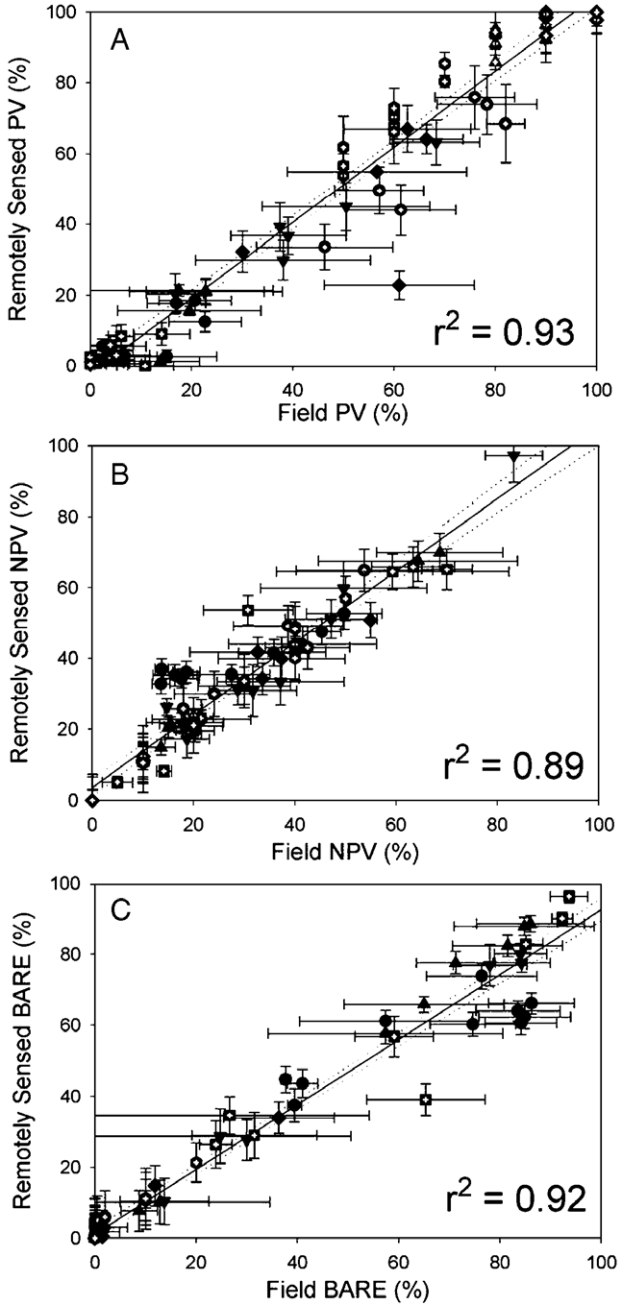

Fig. 7. Field validation of remotely sensed (A) photosynthetic vegetation – PV, (B) non-photosynthetic vegetation – NPV, and (C) bare substrate for areas listed in Table 1 and shown in Fig. 1.

Given that lateral cover fractions can be remotely quantified with reasonable precision and accuracy, it is important to assess whether this measure is unique to previously demonstrated remote sensing measures such as leaf area index (LAI). LAI has been quantified for a number of years using a wide variety of multi-spectral sensors (e.g., Asrar et al., 1986; Myneni et al., 1997). What does imaging spectroscopy offer in terms of vegetation structural analyses that is different from LAI? We used our network of field sites (Fig. 1) to ascertain relationships between LAI and remotely sensed PV+NPV from imaging spectroscopy. PV+NPV was poorly correlated with LAI across the grassland, shrubland, savanna, woodland and forest sites ($r^2=0.46$, $p>0.05$; Fig. 8). Breakdown of the data by ecosystem type or by remotely sensed cover fraction (PV vs. NPV) yielded no substantial change in this relationship (data not shown). The theory behind tied RE-SWIR2 mixture modeling suggests that this new measure should minimize contributions of vertical structure and volumetric changes in leaf area, isolating the horizontal or lateral structure (Asner & Lobell, 2000). This comparison of the imaging spectroscopy results to field-based LAI measurements supports the theoretical basis. Imaging spectroscopy, with tied spectral mixture analysis, appears to isolate a unique structural measure of vegetation.

3.3. Structure by life zone

Compilation of the AVIRIS results by Holdridge life zone highlighted the basic structural differences between systems (Fig. 9). Zones of highest photosynthetic vegetation fractional cover were sub-tropical and lower montane wet forests, with values of 65±11% (s.d.) and 45±2%, respectively. Sub-tropical and lower montane moist forests had similar PV values averaging 36±10% and 34±12%, respectively. PV ranges were much lower in montane wet and moist woodland/forest zones (10–22%), and less than 10% in dry forest, thorn, steppe, and desert zones throughout the image data set. Sub-alpine/alpine zones contained no detectable PV cover. Trends in bare substrate cover among life zones were nearly opposite to those of PV cover, with the lowest values in wet forests (23–28%) and increasing to 100% in sub-alpine/alpine systems (Fig. 9).

The fractional cover of non-photosynthetic vegetation, which is comprised of senescent herbaceous and exposed woody stem material, peaked in sub-tropical dry and thorn forest and lower montane thorn steppe life zones (Fig. 9). The sub-tropical systems had particularly had high NPV cover with relatively low bare substrate exposure, suggesting that these systems are the most fire prone (sensu D'Antonio & Vitousek, 1992; Hughes & Vitousek, 1993). In contrast, upper montane moist and wet forests had relatively high NPV cover values (30–42%), but high bare substrate fractions in the range of 37–58%. As indicated, PV cover was low – averaging 10–22%. Together, these cover fraction results showed that these high-altitude forests have an open, depauperate structure at canopy and regional scales.

These results show that high-fidelity RE-SWIR2 observations provide detailed information on the structure and lateral heterogeneity of diverse ecosystems. Fuel loads, as represented by NPV cover fractions, vary considerably among life zones from about 0% to 80%. Fractional PV cover ranges from zero to nearly 100%. From an ecosystem structural point of view provided by imaging spectroscopy, the Big Island of Hawai'i indeed contains an enormous range of conditions.

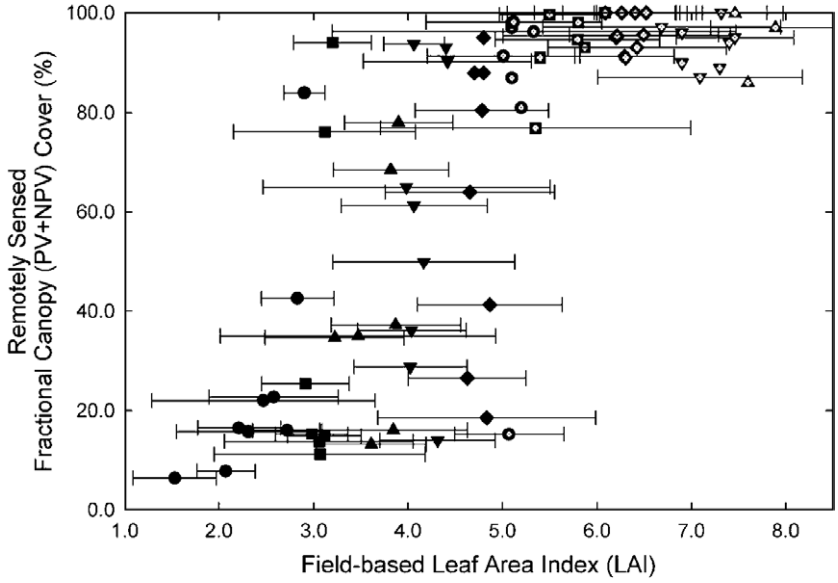

Fig. 8. Relationship between remotely sensed PV+NPV and field-based leaf area index (LAI) measurements. Symbols represent different ecosystem types (Table 1), with highest values from woodlands and forests and lowest values from burned grassland and open shrubland.

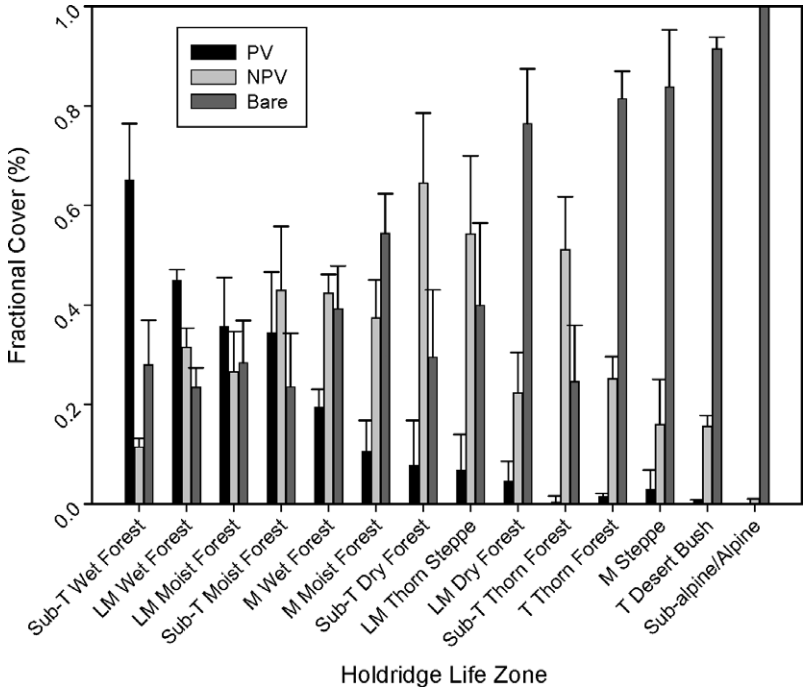

Fig. 9. Remotely sensed fractional cover of PV, NPV and bare substrate by Holdridge life zone. Mean fractional cover is given with error bars showing standard deviation for all AVIRIS pixels in each life zone (as per Table 1).

3.4. Precipitation effects

The regional map of mean annual precipitation (MAP; Fig. 2) was combined with the AVIRIS results to quantify changes in the material composition of ecosystems by rainfall regime (Fig. 10). We found a near-linear 18-fold increase in photosynthetic vegetation fractional cover, as MAP increased from $\leq$250 mm (3.5±1.5%) to 2000 mm (64.5±7.8%). PV cover then declined by 15% from 2000 to 3000 mm MAP. This result suggests that plant growth is not limited by water above 2000 mm year^{-1} rainfall, and it may in fact be limited by water saturation well below reaching 3000 mm year^{-1} (Schuur et al., 2001).

Bare substrate fractional cover decreased precipitously from 50.5±6.7% at $\leq$250 mm MAP to 15.6±5.1% at 1000 mm (Fig. 10). This ~230% decrease was nearly the inverse of the observed PV increase up to 1000 mm MAP. Annual precipitation values above 1000 mm did not result in further declines in bare substrate cover, even at the highest rainfall regime of 3000 mm year^{-1}, where the project-wide

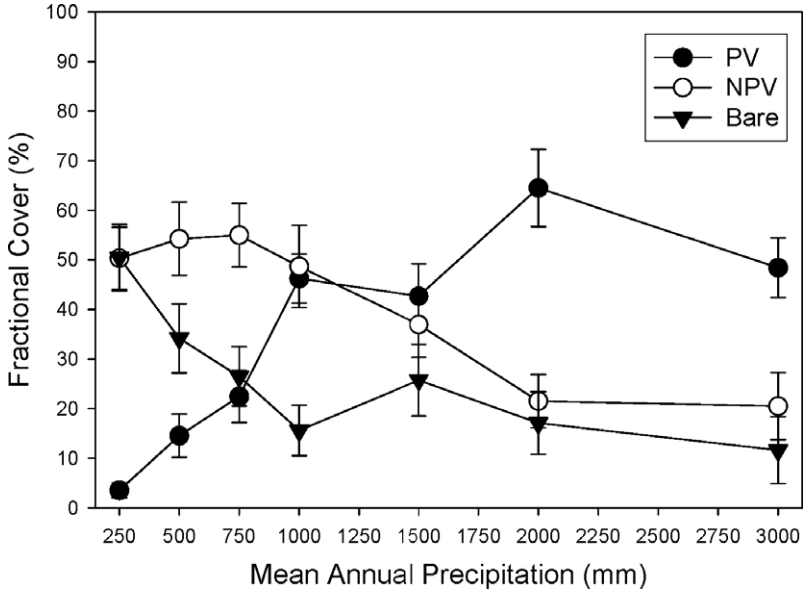

Fig. 10. Remotely sensed fractional cover of PV, NPV and bare substrate by mean annual precipitation. Means and standard deviations are shown for all AVIRIS pixels (as per Table 1).

minimum values were estimated at 11.6±6.1%. Narrow standard error values of 5–7% throughout the precipitation gradient suggest that bare substrate cover variations are weakly determined by vegetation class or land use in Hawai'i. Instead the fraction of exposed soil is foremost climatologically driven and secondarily affected by substrate age (e.g., presence of bare lava flows). The role of open lava fields in determining these relationships might have been greater had we placed emphasis on this source of variation in our remote sensing data collections.

Non-photosynthetic vegetation cover was fairly constant (49–55%) in MAP regimes of ≤250–1000 mm (Fig. 10). NPV declined from 49±8.3% at 1000 mm to 21.5±5.4% at 2000 mm MAP, a 67% average decrease with a doubling of mean annual rainfall. There was no observed trade-off in NPV cover with increasing PV or decreasing bare surface cover at MAP values <1000 mm. NPV did decline in step with increasing green canopy cover in the precipitation range of 1500–2000 mm year^{-1}. There was 20.5±6.8% NPV cover even in the wettest regions of the image collection; these areas were likely openings in the forest canopy that exposed coarse woody debris, standing dead material and/or patches of certain invasive grass species (see previous section). Additional field studies are required to evaluate the accuracy of these findings throughout areas of high rainfall.

As an indicator of fire fuel load, NPV was consistently high when MAP was less than 1500 mm. This range of precipitation values dominated our image collection as it did the entire island (Fig. 2). However, the efficiency of fire spread declines when bare soil fractions increase, serving as important fire breaks (Rollins et al., 2004). Bare substrate cover averaged about 50% in the ≤250 mm rainfall zones found at low elevation on leeward sides of the island's volcanoes (Fig. 10). However, at MAP values of 750–1000 mm year^{-1}, bare substrate fractions were much lower (15–26%) and NPV cover was high (49–55%). These areas are likely the most fire prone and are therefore an important focus for land managers.

4. Conclusions

The Hawaiian Islands contain more than two-thirds of the global life zones delineated by Holdridge (1947). An extraordinary combination of climatic and edaphic variation combined with high biological diversity makes Hawai'i an ideal testing ground for remote sensing studies of ecosystem functioning structure and function.

We tested a fully automated approach for measuring the lateral distribution of plant tissues and bare substrate using high-fidelity imaging spectroscopy and tied shortwave-infrared/red-edge spectral mixture analysis. The method was applied across a wide range of ecological life zones, gradients of mean annual precipitation from ≤250 to >3000 mm year^{-1}, and substrate conditions from bare lava to highly weathered soils. Our findings offer the following conclusions and considerations:

- High-fidelity tied RE-SWIR2 spectroscopy with spectral mixture analysis provides high precision estimates of fractional live and senescent vegetation cover as well as bare substrate cover. These estimates are accurate to levels achieved using time-consuming field and helicopter measurements.
- Remotely sensed fractional cover of photosynthetic and non-photosynthetic vegetation (PV+NPV) is poorly correlated with leaf area index across ecosystem types. This supports the theory that spectral tying minimizes the contribution of vertical structure and volumetric scattering in the measurement, allowing for the isolation of a unique vegetation structural variable.
- The lateral configuration of biological materials is measurably different across a wide range of life zones in Hawai'i. Unique combinations of PV, NPV, and bare substrate quantify fundamental differences in ecosystem structure that serve as a basis for ecosystem monitoring and analysis. These measurements are available at a scale commensurate with field studies and land management efforts.
- There is a near 20-fold increase in PV fractional cover with a 10-fold increase in mean annual precipitation in Hawai'i. This rate of increase asymptotes from 2000 to 3000 mm year^{-1} of rainfall, suggesting that plant growth is not limited by water above 2000 mm year^{-1} and may be limited by water saturation at 3000 mm year^{-1} or less (Schuur et al., 2001).
- NPV fractional cover remains nearly constant at ~50% in ecosystems with mean annual precipitation <1500 mm year^{-1}. Thereafter, it steadily declines to a minimum of ~20% at 3000 mm year^{-1} of rainfall. Bare substrate fractions are highest (~50%) at precipitation levels <750 mm year^{-1}, then decline to <20% in the 750–1000 mm year^{-1} zones. The combination of low bare substrate and high NPV cover in the 750–1000 mm year^{-1} rainfall zones identifies these areas as high fire risk.

The results presented verify the general accuracy, precision and applicability of high fidelity red-edge/shortwave-infrared imaging spectroscopy for ecosystem research on a broader scale. This work also sets the framework for our continued studies of ecosystem structure throughout the Hawaiian Archipelago.

Acknowledgements

We thank H. Farrington, K. Heidebrecht, V. Morris, S. Robinson and B. Sawtelle for logistical and analytical assistance. We thank R. Green, M. Eastwood, and the entire AVIRIS team for their outstanding effort during the flight campaign, and for bringing the highest quality imaging

spectroscopy to the ecological research community. We also thank three anonymous reviewers for their comments on the manuscript. This work was supported by the Carnegie Institution, the Mellon Foundation, and the National Science Foundation (DEB-0136957).

References

Aber, J. D., & Melillo, J. M. (1991). *Terrestrial ecosystems*. Philadephia: Saunders College Publishing.

Adams, J. B., Smith, M. O., & Gillespie, A. R. (1993). Imaging spectroscopy: Interpretation based on spectral mixture analysis. In C. M. Pieters, & P. Englert (Eds.), *Remote geochemical analysis: Elemental and mineralogical composition* (pp. 145–166). New York: Cambridge University Press.

Armstrong, R. W. (Ed.) (1983). *Atlas of Hawaii* (2nd ed.). Honolulu: University of Hawaii Press.

Asner, G. P. (1998). Biophysical and biochemical sources of variability in canopy reflectance. *Remote Sensing of Environment*, *64*, 234–253.

Asner, G. P., & Heidebrecht, K. B. (2002). Spectral unmixing of vegetation, soil and dry carbon cover in arid regions: Comparing multispectral and hyperspectral observations. *International Journal of Remote Sensing*, *23*, 3939–3958.

Asner, G. P., & Heidebrecht, K.B. (2003). Imaging spectroscopy for desertification studies: Comparing AVIRIS and EO-1 Hyperion in Argentina drylands. *IEEE Transactions on Geoscience and Remote Sensing*, *41*, 1283–1296.

Asner, G. P., Keller, M., Pereira Jr., R., Zweede, J. C., & Silva, J. N. M. (2004). Canopy damage and recovery following selective logging in an Amazon forest: Integrating field and satellite studies. *Ecological Applications*, *14*, 280–298.

Asner, G. P., & Lobell, D. B. (2000). A biogeophysical approach for automated SWIR unmixing of soils and vegetation. *Remote Sensing of Environment*, *74*, 99–112.

Asrar, G., Kanemasu, E. T., Miller, G. P., & Weiser, R. L. (1986). Light interception and leaf area estimates from measurements of grass canopy reflectance. *IEEE Transactions on Geoscience and Remote Sensing*, *24*, 76–81.

Bateson, C. A., & Curtiss, B. (1996). A method for manual endmember selection and spectral unmixing. *Remote Sensing of Environment*, *55*, 229–243.

Canfield, R. H. (1941). Application of the line intercept method in sampling range vegetation. *Journal of Forestry*, *39*, 388–394.

Carlson, T. N., & Ripley, D. A. (1997). On the relationship between NDVI, fractional vegetation cover, and leaf area index. *Remote Sensing of Environment*, *62*, 241–252.

D'Antonio, C. M., & Vitousek, P. M. (1992). Biological invasions by exotic grasses, the grass/fire cycle, and global change. *Annual Review of Ecology and Systematics*, *23*, 63–87.

Field, C. B., Randerson, J. T., & Malmström, C. M. (1995). Global net primary production: Combining ecology and remote sensing. *Remote Sensing of Environment*, *51*, 74–88.

Franklin, S. E., & Wulder, M. A. (2002). Remote sensing methods in medium spatial resolution satellite data land cover classification of large areas. *Progress in Physical Geography*, *26*, 173–205.

Giambelluca, T. W., Nullet, M. A., & Schroeder, T. A. (1986). *Rainfall atlas of Hawaii*. Honolulu: Department of Land and Natural Resources, State of Hawaii.

Green, R. O., Eastwood, M. L., Sarture, C. M., Chrien, T. G., et al. (1998). Imaging spectroscopy and the Airborne Visible Infrared Imaging Spectrometer (AVIRIS). *Remote Sensing of Environment*, *65*, 227–248.

Holdridge, L. R. (1947). Determination of world plant formations from simple climate data. *Science*, *105*, 367–368.

Hughes, F., & Vitousek, P. M. (1993). Barriers to shrub reestablishment following fire in the seasonal submontane zone of Hawai'i. *Oecologia*, *93*, 557–563.

Hughes, R. F., Vitousek, P. M., & Tunison, T. (1991). Alien grass invasion and fire in the seasonal submontane zone of Hawai'i. *Ecology*, *72*, 743–746.

Lefsky, M. A., Cohen, W. B., Acker, S. A., Parker, G. G., Spies, T. A., & Harding, D. (1999). Lidar remote sensing of the canopy structure and biophysical properties of Douglas-fir western hemlock forests. *Remote Sensing of Environment*, *70*, 339–361.

Myneni, R. B., Nemani, R., & Running, S. W. (1997). Estimation of global leaf area index and absorbed PAR using radiative transfer models. *IEEE Transactions on Geoscience and Remote Sensing*, *35*, 1380–1393.

Roberts, D. A., Smith, M. O., & Adams, J. B. (1993). Green vegetation, nonphotosynthetic vegetation, and soils in AVIRIS data. *Remote Sensing of Environment*, *44*, 255–269.

Rollins, M. G., Keane, R. E., & Parsons, R. A. (2004). Mapping fuels and fire regimes using remote sensing, ecosystem simulation and gradient modeling. *Ecological Applications*, *14*, 75–95.

Schlesinger, W. H. (1991). *Biogeochemistry: An analysis of global change*. San Diego: Academic Press.

Schuur, E. A. G., Chadwick, O. A., & Matson, P. A. (2001). Carbon cycling and soil carbon storage in mesic to wet Hawaiian montane forests. *Ecology*, *82*, 3182–3196.

Sellers, P. J. (1985). Canopy reflectance, photosynthesis and transpiration. *International Journal of Remote Sensing*, *6*, 1335–1372.

Treuhaft, R. N., & Siqueira, P. R. (2000). Vertical structure of vegetated land surfaces from interferometric and polarimetric radar. *Radio Science*, *35*, 141–177.

Vitousek, P. M., Aplet, G., & Turner, D. (1992). The Mauna Loa environmental matrix: Foliar and soil nutrients. *Oecologia*, *89*, 372–382.

Welles, J. M., & Norman, J. M. (1991). Instrument for indirect measurement of canopy architecture. *Agronomy Journal*, *83*, 818–825.

White, M. A., Asner, G. P., Nemani, R. R., Privette, J. L., & Running, S. W. (2000). Measuring fractional cover and leaf area index in arid ecosystems: Digital camera, radiation transmittance, and laser altimetry methods. *Remote Sensing of Environment*, *74*, 45–57.

Wiemker, R., Rohr, K., Binder, L., Sprengel, R., & Stiehl, H. S. (1996). Application of elastic registration to imagery from airborne scanners. *Proceedings of the International Archives for Photogrammetry and Remote Sensing*, *31*, 1–6.